Current collector-free symmetric μ-supercapacitor based on a ternary composite of graphene, polydopamine and Co 3 O 4

Adnane Bouzina, René Meng, Françoise Pillier, Hubert Perrot, Catherine Debiemme-Chouvy, Ozlem Sel

Current collector-free symmetric µ-supercapacitor based on a ternary composite of graphene, polydopamine and Co_3O_4

Adnane Bouzina[1], René Meng[1], Françoise Pillier[1], Hubert Perrot[1],
Catherine Debiemme-Chouvy[1,*] and Ozlem Sel[2,3,*]

[1] Sorbonne Université, CNRS, Laboratoire Interfaces et Systèmes Electrochimiques, LISE UMR 8235, 4 place Jussieu, F-75005 Paris, France

[2] Chimie du Solide et de l'Energie, UMR 8260, Collège de France, 11 place Marcelin Berthelot, F-75231 Paris Cedex 05, France

[3] Réseau sur le Stockage Electrochimique de l'Energie (RS2E), CNRS FR 3459, 33 rue Saint Leu, F-80039 Amiens Cedex, France

Abstract:

To boost the energy storage of microsupercapacitors (MSCs), a nanocomposite electrode combining carbonaceous materials with metal oxides was developed, i.e. combining capacitive and faradic currents. Our method involves a one-step hydrothermal process, the initial components being graphene oxide, dopamine and Co^{2+} ions, resulting in a reduced graphene oxide-polydopamine-Co_3O_4 composite. Dopamine acts as a reducing agent and prevents graphene oxide agglomeration. Co^{2+} ions are expected to be chelated by polydopamine, likely leading to uniform dispersion of Co_3O_4 particles on the graphene surface. Using this composite as an active material, thin film electrodes were prepared, thoroughly characterized via various chemical techniques, and their electrochemical properties were tested in KOH. In situ electrochemical quartz crystal microbalance was used to elucidate the charge storage process, which showed the presence of a "point of maximum mass" separating a dominant anionic contribution due to the pseudocapacitive response of Co_3O_4 and a cationic contribution reflecting the electroadsorption/desorption of cations on the rGO surface. Lastly, we extended our study to the fabrication of a current collector-free microsupercapacitor device, composed of interdigitated rGO-PDA-Co_3O_4 electrodes, which demonstrates excellent cycling stability over 3000 cycles at a scan rate of 50 $mV.s^{-1}$ and remarkable energy density of 12.25 $mWh.cm^{-3}$ at a power density of 0.26 $W.cm^{-3}$.

Keywords: Graphene, polydopamine, Co_3O_4, EQCM, microsupercapacitor

1. Introduction

Microsupercapacitors (MSCs) are considered to be one of the most important micro-scale power supplies for integrated electronics, due to their prominent features such as light weight, high power density, long-term cycling, and fast charge-discharge capability.[1] Significant improvements have been observed in the nature and composition of main device components (electrodes, electrolyte, current collectors), as well as in the fabrication methods of micro-electrodes (electrodeposition, ink-jet printing, laser-irradiation assisted methods)[1-4], but still facing challenges and require advances in terms of energy density.

Combining carbonaceous materials that store energy electrostatically with metal oxides, storing energy through faradaic reactions, is a promising approach to boost the stored energy densities of MSCs.[5-7] Similar with the traditional supercapacitors, surface or near-surface redox reactions of pseudocapacitive materials lead to an increase in the capacitance of the composite micro-electrode and hence its energy density. Carbonaceous materials, for their part, facilitate the formation of the electrochemical double layer, provide a high-surface-area support for the metal oxides, increase the electrical conductivity and hence the kinetics of redox reactions, along with improving contact between these pseudocapacitive materials and the electrolyte.[7-9]

In this respect, in recent years a wide range of composites of graphene and transition metal oxide/hydroxide, such as RuO_2[10] V_2O_5,[11] NiO,[12] $Ni(OH)_2$,[13] $NiCo_2O_4$,[14] TiO_2,[15] MnO_2[16] and Co_3O_4[17-22] have been investigated as promising electrode materials for supercapacitors. Herein, our choice for the pseudocapacitive material is cobalt oxide (Co_3O_4), which is considered an attractive alternative to replace ruthenium oxide (RuO_2) due to its relatively lower cost, extremely high theoretical capacitance around 3560 $F \cdot g^{-1}$,[23-24] and its availability in various structures and morphologies.[25-29] Hence, many studies have been performed on the synthesis of various cobalt oxide nanostructures for applications in pseudocapacitors. However, reported capacitance values of supercapacitors using Co_3O_4 as electrode material are generally less than 600 $F \cdot g^{-1}$,[30] which is primarily due to the low electrical conductivity of this oxide.[31] To overcome this problem, many composites combining cobalt oxide with other materials such as carbon nanotubes, graphene, conductive polymers, and other metal oxides have been developed.[32-34] The combination of these materials with cobalt oxide mainly aims to improve: (i) the electrical conductivity, (ii) the specific capacitance, (iii) the reversibility of electrochemical reactions and therefore, its coulombic efficiency and cycling stability.

Another issue which should not be disregarded is the mechanical integrity of the electrodes. It is important to note that the volumetric expansion of the metal oxide and the instability of its particles attached to the graphene sheets are likely to lead to detachment of the active material during the charge-discharge process, which will deteriorate the performance of the electrode materials.[32, 35-36] To solve this problem, polydopamine (PDA), obtained by dopamine (DA) oxidation, can be used to improve the adhesion between the pseudocapacitive material particles and the carbon support.[32, 37] Indeed, the catechol group is a good chelating agent for adsorbing a certain amount of metal ions.[38-39] For example, Jiang *et al.*[39] used the chelating ability of polydopamine to immobilize several metal ions, including Nb^{5+}, Ti^{4+}, Zr^{4+}, Ga^{3+}, Y^{3+}, In^{3+}, Ce^{4+}, Fe^{3+}, on polydopamine-coated Fe_3O_4 microspheres.

Herein, we exploited the multifunctional properties of PDA for the preparation and optimization of the reduced graphene oxide-polydopamie-cobalt (II, III) oxide composite (denoted hereafter, rGO-PDA-Co_3O_4) via a one-pot hydrothermal reaction. Firstly, dopamine is used as a reducing agent to reduce graphene oxide (rGO) and self-polymerize on its sheets,[37, 40-41] thereby alleviating the problem of their agglomeration. Subsequently, Co^{2+} ions are expected to be chelated by polydopamine onto the graphene surface, allowing the Co_3O_4 particles to be uniformly dispersed with improved adhesion onto the rGO surface. By this approach, the dissolution of cobalt (II,III) oxide nanoparticles in the electrolyte should be prevented during the electrochemical cycling process. Then, electrodes in the form of thin films were prepared and thoroughly characterized via various (electro)chemical techniques. The charge storage performances were tested in contact with a KOH aqueous electrolyte, prior to the fabrication of an all-solid-state thin film microsupercapacitor (MSC) arrays. For the latter, interdigitated microelectrodes were prepared by laser engraving directly on the plexiglass substrates, leading to a current collector-free MSC. This process is fully compatible with usual microfabrication techniques and offers the possibility of rapid manufacturing and easy control of the geometry of the resulting MSCs (size, shape and number of fingers of the electrodes, size of the inter-electrode spacing) as well as great flexibility of materials and thicknesses to be engraved.[42-44] Finally, the performance of the solid-state symmetric MSC with rGO-PDA-Co_3O_4 interdigitated electrodes and KOH/polyvinyl alcohol (PVA) gel electrolyte were evaluated which has shown enhanced metrics with respect to the state-of-the-art.

2. Results and discussion

2.1 Preparation, morphological and structural characterization of rGO-PDA-Co_3O_4

The rGO-PDA-Co_3O_4 composites were prepared by a hydrothermal route. Pristine Co_3O_4 and binary rGO-Co_3O_4 composites were also synthesized as comparison (see *Experimental Section*). Optimization of the rGO-PDA-Co_3O_4 composition was carried out by monitoring its electroactivity as a function of the graphene oxide/$CoCl_2 \cdot 6H_2O$ ratio (wt%, denoted hereafter as GO/Co(II) ratio) (**Table S1**), while maintaining a previously optimized DA/GO ratio (50 wt%).[45] To do that, a thin layer of the resulting nano-sized powders (**Figure S1**) was coated on conducting substrates, leading to three different rGO-PDA-Co_3O_4 thin film electrodes with various GO/Co(II) ratio. **Figure 1a** shows the cyclic voltammograms obtained for rGO-PDA-Co_3O_4 composites prepared with GO/Co(II) ratios of 5, 10 and 15 wt%, in a 2 M KOH solution and with a potential sweep rate of 50 $mV \cdot s^{-1}$. From these voltammograms, the gravimetric capacitance (GC, in $F \cdot g^{-1}$) of the three rGO-PDA-Co_3O_4 composites was calculated, the results are shown in **Figure 1b**. From this figure, it is clear that the rGO-PDA-Co_3O_4 composite with a GO/Co(II) ratio of 10 wt% has the highest gravimetric capacitance value (708 $F \cdot g^{-1}$ at 50 $mV \cdot s^{-1}$), making it the optimum composition.

To investigate the effect of the presence/absence of PDA on the performances of the material, the rGO-Co_3O_4 composite (reference) was prepared in the same way as the optimal rGO-PDA-Co_3O_4 composite (same GO/Co(II) ratio). **Figure 1c** displays the X-ray diffraction (XRD) profiles of rGO-Co_3O_4 and rGO-PDA-Co_3O_4 films deposited on a glass substrate, subjected to calcination at 500°C. Additionally, XRD patterns of Co_3O_4 powders (with and without calcination) are presented. The analysis reveals that calcination at 500°C for 2 hours significantly enhances the crystallinity of the cobalt (II, III) oxide.

For the three calcined samples Co_3O_4, rGO-Co_3O_4, and rGO-PDA-Co_3O_4 the Bragg reflections observed at 2θ = 19°, 31.27°, 36.85°, 38.57°, 44.85°, 55.66°, 59.39°, and 65.26° correspond to the (111), (220), (311), (222), (400), (511), and (440) planes, respectively. These values align with literature references (JCPDS sheet n°. 42-1467),[46-47] indicating that the Co_3O_4 crystals in these samples have a pure spinel structure. However, the rGO signature is obscured because the high crystallinity of Co_3O_4 dominates the XRD pattern of the ternary composite. Furthermore, thermal gravimetric analysis (TGA) has been performed on the rGO-PDA-Co_3O_4 which reveals that the Co_3O_4 content is 28.6% (**Figure S2**).

The SEM micrographs presented in **Figure S1** show the morphological aspect of the powders of Co_3O_4, rGO-Co_3O_4, and rGO-PDA-Co_3O_4. Analysis of these micrographs reveals a notable

influence of graphene oxide on the hydrothermal synthesis process. The Co_3O_4 powder (**Figure S1a**) exhibits particles with a size exceeding 100 nm. In contrast, the presence of graphene oxide in solution during the hydrothermal synthesis results in a substantial size reduction,

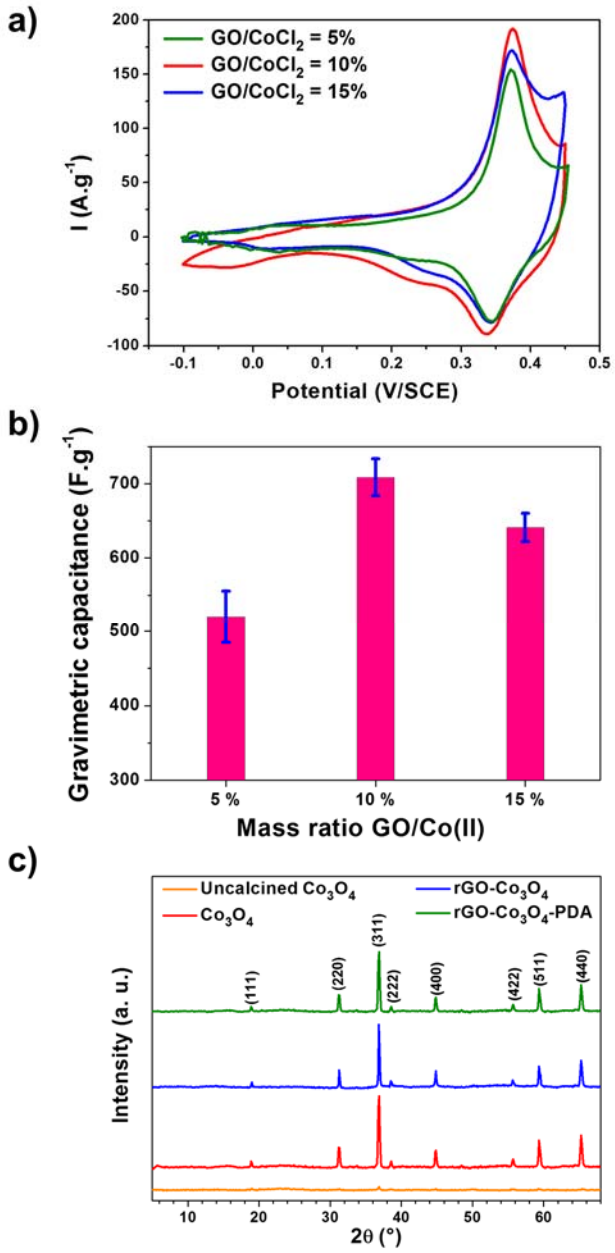

Figure 1. (a) Cyclic voltammograms and (b) gravimetric capacitance of rGO-PDA-Co_3O_4 composites prepared with different GO/$CoCl_2 \cdot 6H_2O$ ratios. CV tests are performed in KOH (2 M) at a scan rate of 50 $mV \cdot s^{-1}$ and the 5th cycle is shown. (c) XRD patterns of the films, corresponding to Co_3O_4 (with)out calcination at 500°C, rGO-Co_3O_4 and rGO-PDA-Co_3O_4.

as evidenced by the SEM micrographs of rGO-Co_3O_4 (**Figure S1b**) and rGO-PDA-Co_3O_4 (**Figure S1c**), where Co_3O_4 particles are observed to be within the range of ~10 nm to ~20 nm. This observation underscores the significant impact of graphene oxide on controlling and minimizing the Co_3O_4 particle size during the synthesis process. Smaller particle size increases electroactive surface area, expected to be beneficial for enhancing cobalt oxide's pseudocapacitive reaction.

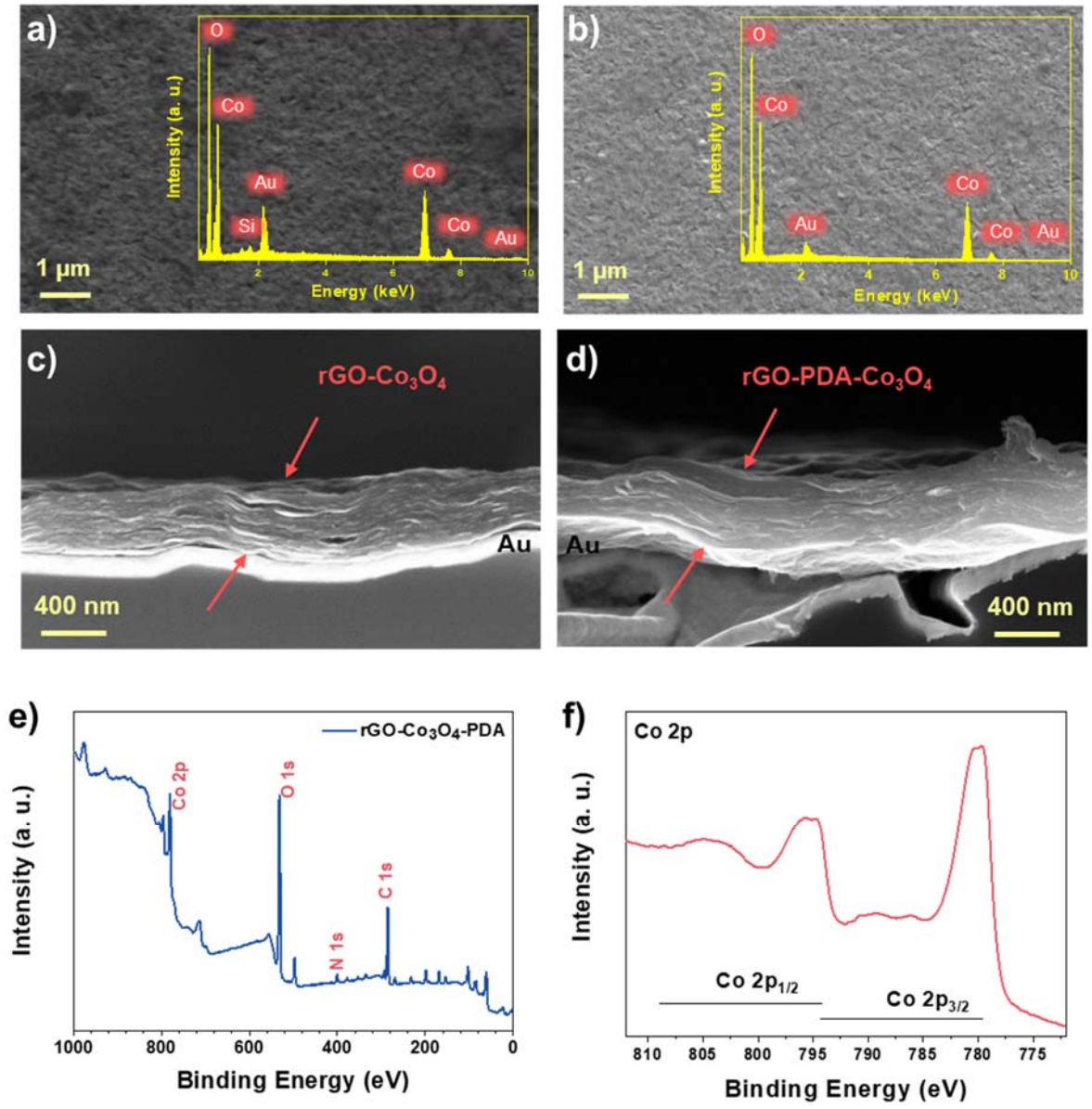

Figure 2. SEM micrographs of the thin film of (a) rGO-Co_3O_4 and (b) rGO-PDA-Co_3O_4 deposited on the Au electrode of a quartz resonator, the corresponding energy dispersive X-ray (EDX) spectra are superimposed, (c) and (d) are the respective cross-section micrographs. XPS analysis of the rGO-PDA-Co_3O_4 film, (e) survey spectrum, (f) high resolution spectrum of the Co2p photopeak.

SEM micrographs in **Figure 2a** and **2b** show the surfaces of rGO-Co_3O_4 and rGO-PDA-Co_3O_4 thin films, deposited on the Au electrode of a quartz resonator and the corresponding energy dispersive X-ray (EDX) spectra are superimposed. To evaluate the spatial arrangement of Co_3O_4 nanoparticles across the surfaces of rGO-Co_3O_4 and rGO-PDA-Co_3O_4 films, EDX maps were generated, permitting the distribution of cobalt to be visualized (**Figure S3**). The results indicate a homogeneous presence of Co_3O_4 nanoparticles on/in both films. **Figure 2c** and **2d** show the cross-section micrographs, thin films with an average thickness of ~380 nm and 430 nm were obtained. Further insights into the chemical composition of the rGO-PDA-Co_3O_4 film were obtained through XPS analysis. **Figure 2e** shows the XPS spectrum obtained for this sample. The C1s peaks of rGO and N1s of PDA are clearly detected around a binding energy of 285 eV and 400 eV, respectively. The high-resolution spectrum of cobalt (Co2p) presented in **Figure 2f**, reveals the presence of two contributions located at 779 and 795 eV corresponding to the Co2p3/2 and Co2p1/2 photopeaks, respectively. These results confirm that this material is a composite of rGO, Co_3O_4 and PDA. To determine the densities of rGO-Co_3O_4 and rGO-PDA-Co_3O_4, these films were first deposited on a quartz electrode of a QCM and their mass was measured. The thicknesses of rGO-Co_3O_4 and rGO-PDA-Co_3O_4 and hence their volumes (given that the surface area of both films is 0.2 cm^2) were then estimated from SEM micrographs of the resonators (**Figure 2c-d**). The average density of both composites is similar, it was estimated at ~1.58 $g{\cdot}cm^{-3}$ and ~1.55·g cm^{-3} for rGO-PDA-Co_3O_4 and rGO-Co_3O_4, respectively (**Table S2**). Following structural and morphological characterizations of the rGO-Co_3O_4 binary composite (reference) and the optimized rGO-PDA-Co_3O_4 ternary composite, the next section will be dedicated to electrogravimetric and electrochemical characterizations in aqueous KOH solution (2 M) to study the effect of the presence of PDA on charge transfer properties at the electrode/electrolyte interface and on charge storage performance.

2.2 Interface analyses of rGO-Co_3O_4 and rGO-PDA-Co_3O_4 by EQCM measurements

The electrogravimetric properties of rGO-Co_3O_4 and rGO-PDA-Co_3O_4 composites were evaluated in a 2 M KOH solution using a three-electrode electrochemical cell, consisting of a quartz electrode covered with rGO-Co_3O_4 or rGO-PDA-Co_3O_4 film as the working electrode. Prior to the use of EQCM under gravimetric mode (*i.e.;* use of Sauerbrey equation[48]), electroacoustic measurements of the rGO-Co_3O_4 and rGO-PDA-Co_3O_4 films were carried out.[49-50] The values obtained for the motional resistance (R_m) and resonant frequency (f) of the quartz electrode without and with the rGO-Co_3O_4 and rGO-PDA-Co_3O_4 films in air and in 2 M

KOH were used to obtain **Figure S4**. In air, the $\Delta R_m/\Delta f$ values of both films lie well on the red line, defining the applicability of the Sauerbrey equation in air. In 2 M KOH solution, the $\Delta R_m/\Delta f$ ratios of both rGO-Co_3O_4 and rGO-PDA-Co_3O_4 films lie between the lower and upper

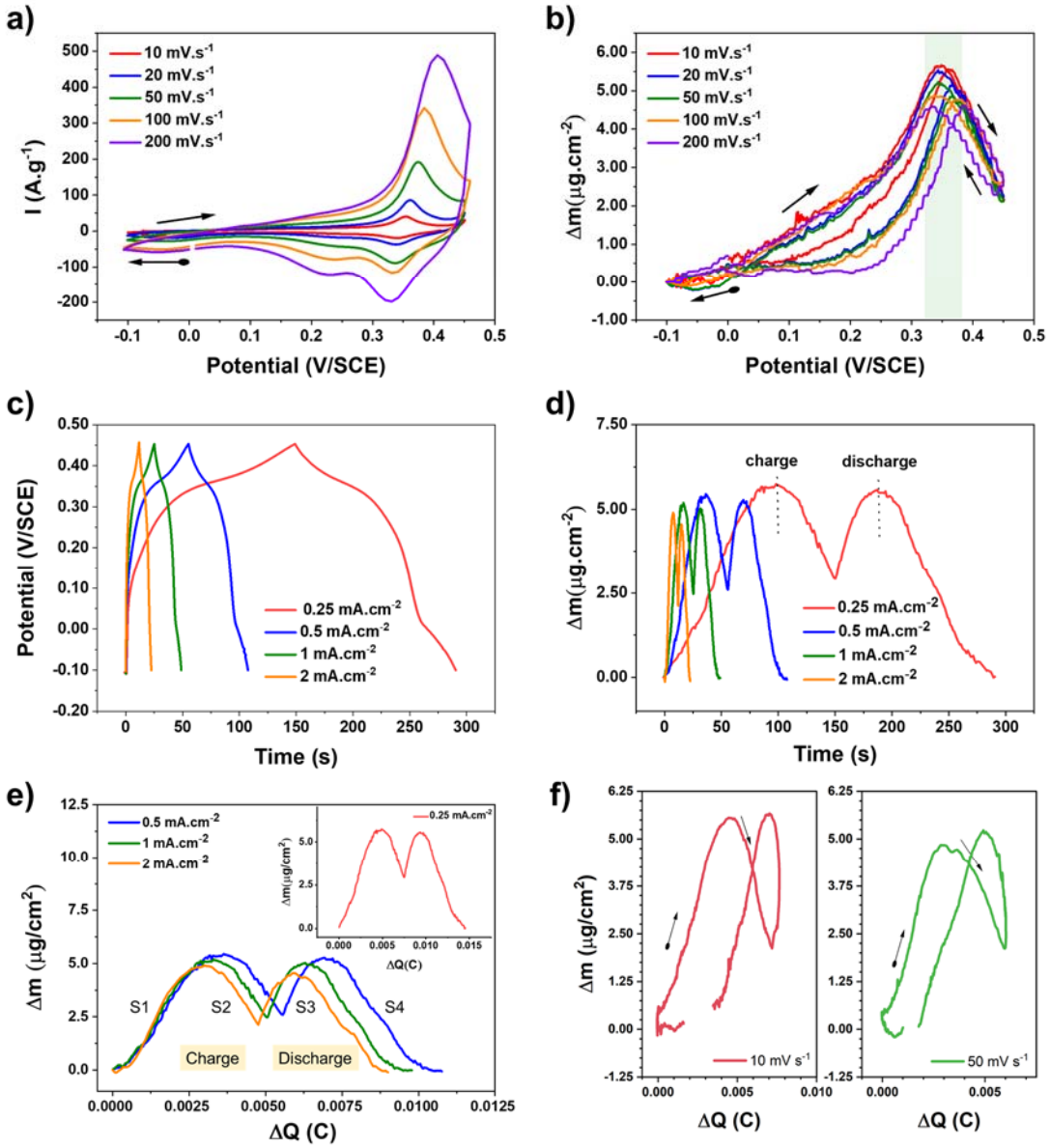

Figure 3. (a) Cyclic voltammograms for rGO-PDA-Co_3O_4 and (b) the corresponding mass variation as a function of potential at different scan rates in KOH 2 M. (c) Potential *versus* time plots and (d) the corresponding mass variation as a function of time, during galvanostatic charge/discharge of rGO-PDA-Co_3O_4 at different current densities, in 2 M KOH. (e) Mass variation as a function of the charge variation of the rGO-PDA-Co_3O_4 composite at different current densities of the GCD-EQCM tests (different slopes are indicated as S1 to S4) and (f) mass variation as a function of the charge variation obtained from the CV-EQCM (only the data obtained at 10 and 50 $mV \cdot s^{-1}$ are shown for clarity).

limits of the gravimetric region (light blue area in **Figure S4**), evidencing that for both rGO-Co_3O_4 and rGO-PDA-Co_3O_4 composites, the microbalance operates under the gravimetric regime.[48-51]

Characterization of the rGO-Co_3O_4 and rGO-PDA-Co_3O_4 films was first carried out using the QCM coupled to cyclic voltammetry (**Figure S5** and **Figure 3**, respectively). **Figure S5a** and **3a** show the CV curves of rGO-Co_3O_4 and rGO-PDA-Co_3O_4, respectively, at different potential scan rates. Each curve shows well-defined pair of redox peaks, indicating that the electrode has pseudocapacitive properties. According to the literature,[17, 27, 32] these redox peaks are attributed to the pseudocapacitive behavior of Co_3O_4, which can be explained by a two-step charge transfer process following the electrochemical reactions below:[52]

$$Co_3O_4 + OH^- + H_2O \leftrightarrows 3\ CoOOH + e^- \quad (1)$$

$$CoOOH + OH^- \leftrightarrows CoO_2 + H_2O + e^- \quad (2)$$

Increasing scan speed results in an increase of the current density corresponding to these redox peaks and a slight shift of the cathodic and anodic peaks towards more negative and positive potentials, respectively, due to the increase in internal resistance.[32] The small inter-peak gap (ΔE_p) even at relatively fast scan rates (100 and 200 mV s^{-1}) (**Figure 3a**) suggests that for both composites electron transfer occurs rapidly.[32] At a scan rate of 100 mV·s^{-1}, the potential gap between the anodic and cathodic peaks (ΔE_p) for rGO-Co_3O_4 and rGO-PDA-Co_3O_4 is 62 mV and 48 mV, respectively, revealing improved electron transfer for the PDA-containing composite. In addition, the higher normalized current observed in CV responses for the rGO-PDA-Co_3O_4 composite compared with rGO-Co_3O_4 (**Figure 3a** and **S5a**) may indicate an improved accessibility to the redox-active sites of rGO-PDA-Co_3O_4.

Figure 3c and **S5c** show galvanostatic charge-discharge curves at different current densities of the rGO-Co_3O_4 and rGO-PDA-Co_3O_4 composites, respectively. They show typical pseudo-capacitive behavior, with a quasi-horizontal plateau over the potential range 0.25 to 0.35 V *vs.* SCE. For a given current density, the plateau potential is virtually identical at charge and discharge. This is in good agreement with the small inter-peak distance observed by cyclic voltammetry.

The mass variations obtained simultaneously during the CV and GCD which are associated with charge transfer processes at the electrode/electrolyte interface are plotted in **Figure S5b, S5d** for rGO-Co_3O_4 and in **Figure 3b, 3d** for the rGO-PDA-Co_3O_4 composites, respectively. It

is clear from the CV coupled QCM analysis that the mass variations of the two electrodes show a sudden change in slope at around 0.325 to 0.375 V/SCE (varies depending on the scan rate) both during positive and negative potential scan of the potential (**Figure 3b** and **S5b**). Indeed, for potentials more cathodic than this point, the mass of both films increases during Co_3O_4 oxidation and decreases during reduction. This indicates, a priori, that OH^- anions play a predominant role in charge compensation during this process. This result is rather consistent with the pseudocapacitive nature of Co_3O_4. Whereas for more anodic potentials than this point, the mass of both electrodes increases and decreases during cathodic and anodic scan, respectively. This may indicate that cations play a dominant role on the charge storage process, which is probably due to the electroadsorption/desorption of cations on the active rGO surface. It is noted that a Δm slope change is also observed within the charge and discharge process during the GCD-QCM analysis (**Figure 3d** for the rGO-PDA-Co_3O_4 and **Figure S5d** for the rGO-Co_3O_4), in line with the above hypothesis.

To test this hypothesis and obtain indications of the nature of the species transferred, the Δm *versus* ΔQ curves were plotted, where mass per electron (M.P.E.) is estimated by $\frac{M.P.E.}{n} = \mathrm{F}\frac{\Delta m}{\Delta Q}$ (n, number of electrons transferred and F, Faraday's number). **Figure 3e** shows Δm *versus* ΔQ plots from the GCD tests of the rGO-PDA-Co_3O_4 composite, which shows 4 different slopes (S1-S4). The responses obtained from the tests at different current densities show similar behavior with comparable slopes, except slightly smaller values were obtained at 0.25 $mA \cdot cm^2$ (inset of **Figure 3e**). The evolution of the M.P.E. during charge presents two distinct domains. The first one extends up to 3 mC, with an estimated $M.P.E._{S1}$ of 37 $g \cdot mol^{-1}$. This phase probably corresponds to a process with a main participation of the OH^- anions and H_2O molecules, in agreement with reaction 1 and 2. As the charge process proceeds, a slope change (from 3 mC to 5 mC), with an average $M.P.E._{S2}$ of -30 $g.mol^{-1}$, which can be attributed to the contribution of the K^+ cations, which prevails over the OH^- dominant pseudocapacitive charge compensation process. During discharge, the same trend is observed with comparable M.P.E. values, indicating the reversibility of this process. To substantiate these findings, M.P.E. values from the CV-QCM data of **Figure 3a** and **3b** were also estimated. **Figure 3f** shows the Δm *versus* ΔQ plots for two different scan rates of the potential. At 50 $mV \cdot s^{-1}$, during the anodic scan, a M.P.E. of 30 $g.mol^{-1}$ was estimated corresponding to a main participation of anionic species which was then followed by a M.P.E. of -26 $g.mol^{-1}$, indicating a major cationic response. At 10 $mV \cdot s^{-1}$, the same trend is observed, with slightly smaller values. Overall, EQCM analysis highlights the competition between an OH^- dominant charge compensation process due to the

pseudocapacitive response of Co_3O_4 and a cationic contribution reflecting the electroadsorption/desorption of K^+ species on the rGO surface.

2.3 Charge storage performance of rGO-Co_3O_4 and rGO-PDA-Co_3O_4 composite in KOH

In order to correlate the properties of the PDA with the electrochemical performance of the rGO-PDA-Co_3O_4 composite, the capacitive performances of the thin film electrodes were investigated by cyclic voltammetry at different scan rates. **Figure 4a** and **4b** report the gravimetric and volumetric capacitance of the rGO-Co_3O_4 and rGO-PDA-Co_3O_4 composites, respectively (from 10 $mV \cdot s^{-1}$ to 200 $mV \cdot s^{-1}$, calculated from the CV curves in **Figure 3a** and **Figure S5a**). The rGO-PDA-Co_3O_4 composite has higher gravimetric and volumetric capacitance than rGO-Co_3O_4. At a scan rate of 10 $mV \cdot s^{-1}$, rGO-PDA-Co_3O_4 has a gravimetric capacitance of 851 $F \cdot g^{-1}$ and a volumetric capacitance of 1345 $F \cdot cm^{-3}$ *versus* 594 $F \cdot g^{-1}$ and 904 $F \cdot cm^{-3}$ for rGO-Co_3O_4, *i.e;* an increase about 50% of the composite electrochemical response in the presence of PDA that is on or between the sheets of rGO. PDA enables, on one hand, a decrease of agglomeration of the latter, likely resulting in a greater active surface compared to rGO-Co_3O_4. On the other hand, it facilitates the uniform dispersion and a high content of Co_3O_4 nanoparticles on the rGO sheets due to PDA's chelation properties. Additionally, the rGO-PDA-Co_3O_4 composite electrode has a significant capacitance retention with respect to increased scan speed (from 10 $mV \cdot s^{-1}$ to 200 $mV \cdot s^{-1}$) (**Figure 4a** and **4b**). The volumetric capacitance of the rGO-PDA-Co_3O_4 composite changes from 1345 $F \cdot cm^{-3}$ to 856 $F \cdot cm^{-3}$, i.e. a drop of only 36% against a drop of 50% for rGO-Co_3O_4 (the latter presents 904 $F \cdot cm^{-3}$ at 10 $mV \cdot s^{-1}$ and 453 $F \cdot cm^{-3}$ at 200 $mV \cdot s^{-1}$). This finding suggests a rapid charge transfer inside the rGO-PDA-Co_3O_4 nanocomposite compared to rGO-Co_3O_4.

To elaborate further this point, EIS analyses were performed. **Figure 4c** and **4d** present the Nyquist plots of the two composites rGO-PDA-Co_3O_4 and rGO-Co_3O_4 at 0.32 V/SCE and 0.4 V/SCE (see CV curves in **Figure 3**). These potentials were chosen to represent two different regions revealed in the EQCM analysis (*i.e.,* lower and higher potentials than the maximum observed in the Δm response in **Figure 3b**). In the high frequency region, a semicircle is present in the Nyquist diagrams. This semicircle is attributed to the charge transfer resistance (R_{ct}) at the interface between the electrode and the electrolyte. The R_{ct} values estimated by fitting the semicircle of the Nyquist diagrams (**Figure 4c-d**) and reported in **Table 1**. The low R_{ct} values obtained for rGO-PDA-Co_3O_4 compared to rGO-Co_3O_4 suggest faster charge-discharge kinetics

and therefore plausibly higher power performance for the rGO-PDA-Co_3O_4 composite. At low frequencies, a clear increase in the imaginary part of the impedance is observed for the two

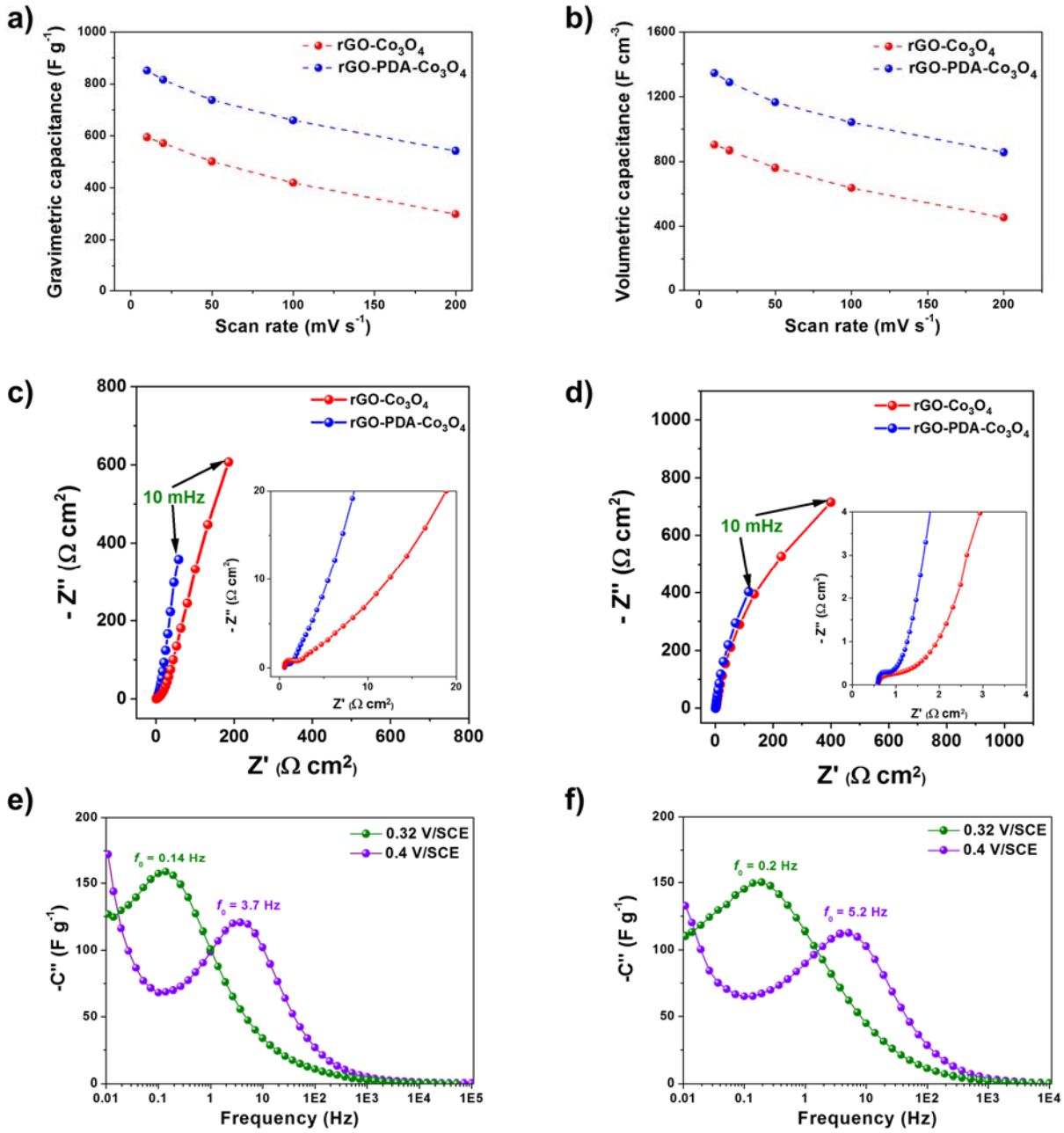

Figure 4. Evolution of (a) the gravimetric capacitance and (b) the volumetric capacitance of rGO-Co_3O_4 and rGO-PDA-Co_3O_4 as a function of the scan rate. Nyquist diagrams of rGO-Co_3O_4 and rGO-PDA-Co_3O_4 at a potential of (c) 0.32 V/SCE and (d) 0.4 V/SCE in 2 M KOH. Evolution of the imaginary part (C'') of the capacitance as a function of the frequency at two potentials 0.32 V/SCE and 0.4 V/SCE for (e) rGO-Co_3O_4 and (f) rGO-PDA-Co_3O_4.

Table 1. EIS data, charge transfer resistance ($\Omega \cdot cm^2$) and time constant (s) determined for rGO-Co_3O_4 and rGO-PDA-Co_3O_4 at 0.32 and 0.4 V/SCE in 2 M KOH solution.

	Transfer resistance ($\Omega \cdot cm^2$)		Time constant (s)*	
	Potential (V vs SCE)			
Electrode	*0.32 V*	*0.40 V*	*0.32 V*	*0.40 V*
rGO-Co_3O_4	1.3	0.9	7.1	0.27
rGO-PDA-Co_3O_4	0.8	0.5	5	0.19

* $\tau_0 = 1/f_0$

studied potentials (0.32 and 0.4 V/SCE), forming a slightly inclined straight line at low frequencies which indicates the contribution of multiple ionic species in the charge compensation process. This is in agreement with the EQCM results (**Figure 3**). To determine the time constants (τ_0), characteristic of the rapidity of the electrode response, the imaginary part of the capacitance C"(ω) and the relaxation time which corresponds to the peak frequency (f_0) of the C"(ω) curve were calculated, for the two potentials, following **Equation S3** and **S4**. The average time constants obtained from C"(ω) curves (**Figure 4e** and **4f**) are summarized in **Table 1**. At a given potential, the rGO-PDA-Co_3O_4 composite exhibits a lower τ_0 than that of rGO-Co_3O_4 (5 s against 7.1 s at 0.32 V/ECS and 0.19 s against 0.27 s at 0.4 V/ECS) indicating that it has faster kinetics during charge-discharge process. This result is consistent with better capacitance retention as a function of scan rate of the composite (rate performance) with PDA (64%) compared to the composite without PDA (50%) (**Figure 4a** and **4b**).

It is also noted that for a given composite the time constants obtained at 0.32 V/SCE (lower than the maximum observed in Δm response in **Figure 3b**) and 0.4 V/SCE (higher than the maximum observed in Δm response in **Figure 3b**) are very different. Indeed, for the two electrodes the time constants at 0.32 V/SCE are greater compared to those obtained at 0.4 V/SCE (**Table 1**). This indicates that the charge storage at 0.32 V/SCE is mainly due to a phenomenon with slower kinetics, which is in line with the pseudocapacitive reactions of Co_3O_4. Accordingly, at 0.4 V/SCE, the observation of smaller τ_0 suggests a rapid phenomenon of charge storage and electro-adsorption/desorption of cations as the predominant mechanism. This result confirms our explanation of the EQCM response.

The cycling stability of rGO-Co_3O_4 and rGO-PDA-Co_3O_4 was investigated by CV (**Figure 5** and **S6**) at a scan rate of 50 $mV \cdot s^{-1}$ in 2 M KOH. The rGO-PDA-Co_3O_4 composite exhibits

outstanding stability, showcasing an impressive capacitance retention of 97% after 3000 cycles with a coulombic efficiency of ~85% (**Figure 5**). In contrast, the rGO-Co_3O_4 film displays a capacitance retention of 90% (**Figure S6**). In addition, a loss of 10% of the active material was detected (estimated by QCM) after the 3000 cycles for the rGO-Co_3O_4 against less than 1% for the composite containing the polydopamine. This can be explained by the dissolution of Co_3O_4 nanoparticles due to poor adhesion between Co_3O_4 and rGO sheets for the rGO-Co_3O_4 composite. To confirm that this loss is due to the poor mechanical behavior in solution of the rGO-Co_3O_4 composite, polyvinylidene fluoride (PVDF) was used as a binder for the rGO-Co_3O_4.

The study of the cyclability of the rGO-Co_3O_4-PVDF composite material, carried out over 3000 cycles at a scan rate of 50 $mV \cdot s^{-1}$ (**Figure S6c**) reveals a loss of only 5% of the initial capacitance. This can indicate an improvement of the mechanical strength of the electrode due to the presence of PVDF. However, the electrochemical response of rGO-Co_3O_4-PVDF is still weaker than that of rGO-PDA-Co_3O_4 (**Figure S6d**), thus the capacitance values are significantly enhanced when PDA is present in the composite electrode. This result highlights the multifunctional role of PDA within the rGO-PDA-Co_3O_4 composite. Indeed, PDA not only facilitates the uniform dispersion of Co_3O_4 nanoparticles with a high content on the rGO surface, but also serves as a binder, enhancing the mechanical strength of the electrode and thereby preventing the dissolution of Co_3O_4 nanoparticles in the electrolyte.

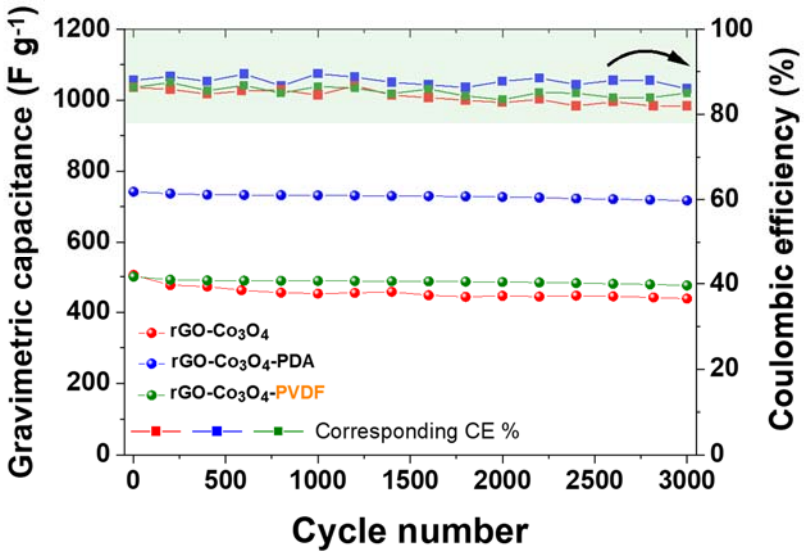

Figure 5. Gravimetric capacitance (left) and coulombic efficiency (right) *vs.* cycle number of rGO-Co_3O_4, rGO-PDA-Co_3O_4 and rGO-Co_3O_4-PVDF composite, at a scan rate of 50 $mV \cdot s^{-1}$.

2.4 Solid state current collector free symmetric microsupercapacitor based on rGO-PDA-Co_3O_4

The rGO-PDA-Co_3O_4 composite thin film electrode has presented a superior performance at a liquid electrolyte interface in a 3-electrode cell. As a next step, its suitability as electrode material in a solid state symmetric MSC device was tested. It is noted that rGO-PDA-Co_3O_4 has been prepared in a hydrothermal route which facilitates the device fabrication. Since the electrode fabrication does not require a conducting substrate, unlike electrochemically prepared reduced graphene oxide and PDA based composites,[53] it is possible to fabricate a current-collector free symmetric μ-supercapacitor device. A slurry containing the rGO-PDA-Co_3O_4 composite was deposited onto a plexiglas substrate which was then patterned into interdigitated electrodes by laser carving. SEM micrograph of the rGO-PDA-Co_3O_4 MSC is shown in **Figure 6a**. The size of the interdigitated patterns and the inter-electrode spacing are 500 μm and 200 μm, respectively and the rGO-PDA-Co_3O_4 film thickness is about 650 μm (**Figure 6a** and **6b**). It is also obvious that the material has been perfectly etched from the inter-electrode spacing, which ensures the absence of a short circuit in the cell, which is assembled in a symmetric configuration and using KOH/polyvinyl alcohol (PVA) gel electrolyte.

Figure 6c shows the voltammograms obtained for the rGO-PDA-Co_3O_4 MSC across a range of scan rates from 10 $mV \cdot s^{-1}$ to 200 $mV \cdot s^{-1}$. Remarkably, the current densities attained at a given scan rate surpass those of ERGO-PDA and rGO-PDA MSCs, reported in our previous work.[45, 53] This elevated performance is attributed to the pseudocapacitive contribution arising from the presence of cobalt oxide (Co_3O_4).

The volumetric capacitances of the MSC were deduced from the galvanostatic charge-discharge curves (**Figure 6d**) depicted in **Figure 6e**. These experiments were conducted at various current densities within a potential range of 0.7 V. It is obvious from the results that the rGO-PDA-Co_3O_4 MSC exhibits remarkable capacities. At a current density of 0.052 $mA \cdot cm^{-2}$, the rGO-PDA-Co_3O_4 MSC achieves a capacitance of 180 $F \cdot cm^{-3}$, exceeding the capacitance values observed in MSCs utilizing capacitive materials under comparable current densities.[45, 53] However, the capacitance of the rGO-PDA-Co_3O_4 micro-device decreases significantly when the current density increases, reaching 41% of the initial capacitance (at 0.052 $mA \cdot cm^{-2}$) for a current density 20 times greater (1 $mA \cdot cm^{-2}$). This decline can be attributed to the sluggish kinetics of pseudocapacitive reactions involving Co_3O_4.

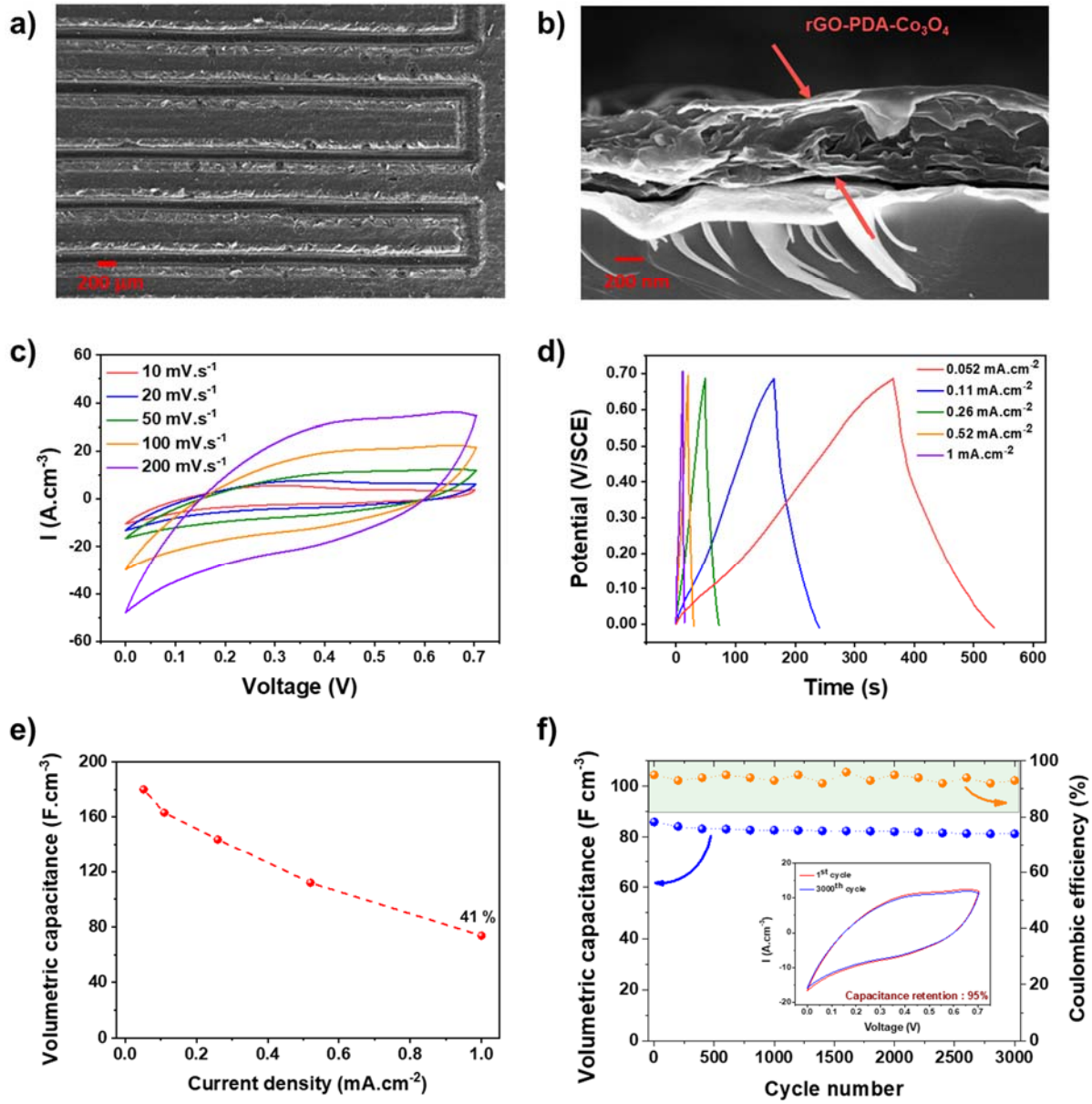

Figure 6. SEM micrographs of (a) the top view and (b) the cross-section of an rGO-PDA-Co_3O_4 interdigitated electrode. (c) Cyclic voltammograms at different scan rates and (d) galvanostatic charge-discharge curves at different current densities. (e) Volumetric capacitance as a function of the current density of the rGO-PDA-Co_3O_4 MSC. (f) Cycling stability of rGO-PDA-Co_3O_4 MSC (3000 cycles at 50 $mV \cdot s^{-1}$).

The cyclability of rGO-PDA-Co_3O_4 MSC was evaluated over 3000 cycles of cyclic voltammetry performed over a potential window of 0.7 V at a scan rate of 50 $mV \cdot s^{-1}$ (**Figure 6f**). A capacitance retention of 95% after the 3000 cycles and over 92% CE, highlighting its remarkable stability over extended cycling.

The rGO-PDA-Co_3O_4 MSC performance in relation to the state-of-the-art is illustrated in **Figure 7** that shows a Ragone plot. Specific energy densities and specific power densities were obtained from the galvanostatic charge/discharge curves according to **Equation S5** and **S6**. The rGO-PDA-Co_3O_4 MSC is capable of delivering higher or equivalent energy densities compared to the reported performance of micro-supercapacitors using pseudocapacitive electrodes.[54-60] Indeed, at a power density of 0.26 $W \cdot cm^{-3}$, the rGO-PDA-Co_3O_4 MSC developed in this work can provide an energy density of 12.25 $mWh \cdot cm^{-3}$. For high power densities, the volumetric energy densities delivered by the rGO-PDA-Co_3O_4 MSC become comparable to those delivered by the MSCs based on ERGO-PDA and rGO-PDA,[45, 53] due to the low kinetics of the pseudocapacitive reactions of Co_3O_4. These results indicate that the rGO-PDA-Co_3O_4 MSC is rather suitable for applications that require moderate power densities with high energy densities.

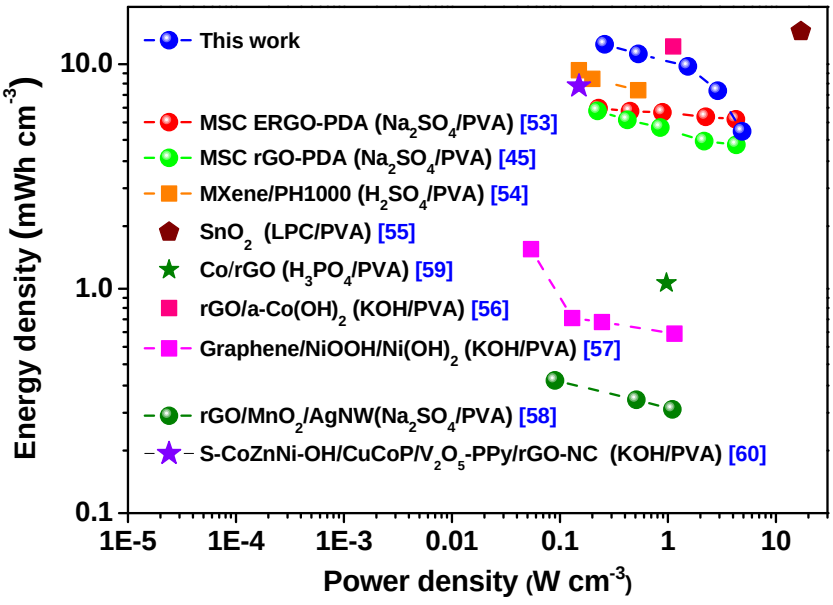

Figure 7. Ragone plot positioning the rGO-PDA-Co_3O_4 µ-device over other reports in the literature.

3. Conclusions

This work focuses on the elaboration of a ternary composite rGO-PDA-Co_3O_4 through a hydrothermal process and its performance evaluation as an active material for supercapacitor devices. The rGO-PDA-Co_3O_4 composite was optimized by varying the GO/$CoCl_2$•$6H_2O$ ratio. It was found that the composite corresponding to an initial GO/Co(II) mass ratio of 10% has the highest gravimetric capacitance (708 $F \cdot g^{-1}$ at 50 $mV \cdot s^{-1}$), making it the optimum composition. The spinel structure of Co_3O_4 was confirmed by XRD and the presence of PDA was shown by XPS and EDX. First, the multifunctional role of PDA in the rGO-PDA-Co_3O_4 composite has been demonstrated by the various electrochemical (CV, GCD, EIS) and electrogravimetric (EQCM) analyses in aqueous liquid electrolyte by comparing the composites with and without PDA. The EQCM data revealed a distinct "point of maximum mass" indicating the differentiation between an anion dominant process associated with the pseudocapacitive behavior of Co_3O_4 and a cation dominant counterpart related to the electroadsorption/desorption of cations onto the surface of reduced graphene oxide (rGO). Compared to the composite without PDA, rGO-PDA-Co_3O_4 has (i) better rate performance (higher capacitance retention with increased scan rates) and (ii) high gravimetric and volumetric capacitance, suggesting an enhanced electro-active surface for charge storage and a significant contribution of pseudocapacitance due to the accessible Co_3O_4 content. The rGO-PDA-Co_3O_4 composite material also showed good cycling stability attributed to an improvement in the mechanical strength of the composite electrode thanks to the adhesive properties of PDA which helps to significantly reduce the dissolution of the active material in the electrolyte. This finding is correlated to the fact that Co^{2+} ions could be chelated by polydopamine onto the graphene surface, allowing the Co_3O_4 particles to be uniformly dispersed with improved adhesion onto the rGO surface.

Next, we have shown the suitability of optimized rGO-PDA-Co_3O_4 nanocomposite as an electrode material in MSC devices. A thin film rGO-PDA-Co_3O_4 on plexiglas was patterned into interdigitated electrodes by laser carving. Interdigitated electrodes were assembled using KOH/PVA gel electrolyte, enabling a current collector-free symmetric μ-supercapacitor device. High capacitance and therefore high energy density was reached with notable power performance due to a fine balance of between Co_3O_4 and rGO, thus between the pseudocapacitive contribution and the high surface area for electroadsorption/desorption process. The μ-device also shows a significant cycling stability of 3000 cycles, which was attributed to the presence of polydopamine in the composite material, providing mechanical

integrity to the electrode. Overall, our study presents a rGO-PDA-Co_3O_4 nanocomposite based solid state MSC device with a remarkable energy density of 12.25 mWh.cm^{-3} at a 0.26 W.cm^{-3}. It is believed that the presented strategy will provide numerous opportunities for developing composite materials with other metal oxides, hydroxides with enhanced mechanical integrity. Furthermore, our current studies indicate the possibility of fabricating devices on flexible substrates, such as polyethylene terephthalate (PET) which exhibits remarkable performance when bent, thereby suggesting the potential application of this work in wearable electronics.

4. Experimental section:

Materials:

Synthesis and electrode preparation: In 15 mL of a GO suspension (at 1 mg·mL^{-1}), 30 mg of dopamine (corresponding to a GO/DA ratio of 50 wt%, as optimized in our prior work)[45], 66.7 mg of Tris (0.1 M Tris, pH=8.5) and 3 different quantities of cobalt chloride hexahydrate, $CoCl_2 \cdot 6H_2O$, (0.3, 0.15 and 0.1 g) were solubilized (**Table S1**). The pH of the mixture was adjusted to 7 by adding a few drops of hydrochloric acid (HCl). After 30 minutes in an ultrasonic bath, the suspension was placed in a Teflon-lined autoclave (25 mL volume) and heated to 200°C for 8 h. Co_3O_4 was also prepared for comparison reasons, the hydrothermal reaction was carried out in the same way ($CoCl_2 \cdot 6H_2O$ was solubilized in Tris solution) but in the absence of dopamine and graphene oxide.

After hydrothermal treatment, a black powder was recovered by vacuum filtration and rinsed several times with ethanol followed by double-distilled water. This powder was then calcined under air at 500°C for 2 h (to improve Co_3O_4 crystallinity). After the thermal treatment, the powder was ground in a mortar and suspended in bidistilled water (2 mg·mL^{-1}) to prepare the ink used to make rGO-Co_3O_4 and rGO-PDA-Co_3O_4 films. The ink was homogenized using an ultrasonic probe, while keeping the sample (ink) in an ice bath (to avoid overheating).

For the electrogravimetric and electrochemical characterization, 6 µL of the rGO-Co_3O_4 or rGO-PDA-Co_3O_4 suspension (2 mg·mL^{-1} in bidistilled water) were deposited on the gold electrode of the quartz resonator (AWS-Sensors, Spain) (Au electrode surface of 0.2 cm^2). The rGO-Co_3O_4 or rGO-PDA-Co_3O_4 films were obtained after a drying step at 70°C in an oven for 30 min. The mass of the film deposited on the quartz electrode was estimated from its frequency variation (bare resonator and after film deposition) in air using the well-known Sauerbrey equation.[48]

A rGO-Co_3O_4-PVDF electrode was also prepared as comparison. 18 mg of ground rGO-Co_3O_4 (90%) and 2 mg of PVDF were dispersed in 10 mL of N-methyl-2-pyrrolidone (NMP), leading to 2 mg·mL^{-1} of rGO-Co_3O_4-PVDF in NMP. To prepare the rGO-Co_3O_4-PVDF film, 6 µL of the rGO-Co_3O_4-PVDF suspension were deposited on the electrode then dried at 90°C in an oven for 30 min.

Electrochemical and Electrogravimetric Characterizations: The electrochemical and electrogravimetric characterizations were carried out using a standard three electrode configuration with an Autolab potentiostat (Metrohm, France). The gold (Au) electrode of quartz resonator (S = 0.2 cm^{-2}) (AWS-Sensors, Spain) modified by the electrode materials introduced above were used as the working electrode, a platinum grid and a saturated calomel electrode (SCE) were used as counter electrode and reference electrode, respectively.
For the classical EQCM analysis, a lab-made QCM coupled with an Autolab potentiostat (PGSTAT12) was used. Under the gravimetric regime, the mass variation, Δm, was obtained from Δf by using of the Sauerbrey equation, $\Delta f = -k_s \times \Delta m$, where k_s is the experimental mass sensitivity constant which has a value of 16.3 Hz·cm^2·g^{-1} for 9 MHz AT-cut QCM.[61]

Morphological and Compositional Characterizations: Morphological observations were done under a field emission gun scanning electron microscope (FEG−SEM) (Ultra55, Zeiss) operating at 10 kV. XPS analyses were performed using an Omicron Argus X-ray photoelectron spectrometer with monochromatized Al Kα excitation (1486.6 eV) with band-pass energies of 100 and 20 eV for acquisition of the survey and high-resolution spectra, respectively. For the XPS analyses, the films were prepared on a gold-coated mica substrate. XRD was performed using a Philips PANalytical X'Pert Pro diffractometer with Cu Kα radiation (λ = 1.54184 Å). The samples were prepared on a glass substrate. Thermogravimetric analysis (TGA) of the powder was performed using a TGA 550 from TA Instruments, under air atmosphere, with a heating rate of 10°C·min^{-1}.

Preparation and electrochemical tests of the rGO-PDA-Co_3O_4 MSC: 150 µL of a suspension of rGO-PDA-Co_3O_4 (2 mg·mL^{-1}) were deposited on the engraved part of a plexiglass substrate (2 cm^2 portion was etched using a laser cutter (Trotec SP500, CO_2 laser)), and dried at 70°C in an oven. Subsequently, the interdigital patterns were obtained by removing the unwanted areas of material (interdigitated finger spacing) by CO_2 laser to obtain a desired pattern, which is instructed through the software Trotec JobControl®. The laser power, scan rate and pulse duration were set to 35 W and 35 cm·s^{-1} and 1.25 ms, respectively. Electrochemical

characterization of the all-solid-state rGO-PDA-Co_3O_4 device was performed with a KOH/PVA gel electrolyte. The gel electrolyte was prepared by solubilizing 0.25 g of KOH and 0.25 g of PVA in 2.5 mL of bidistilled water. The mixture was heated to 80°C under vigorous stirring until the solution became homogeneous. A drop of the mixture was then deposited on the interdigital electrodes. Finally, drying was carried out in air overnight. After electrical connections, symmetric all-solid-state MSC was tested using Cyclic Voltammetry (CV) and Galvanostatic Charge/Discharge (GCD), using an Autolab potentiostat (PGSTAT12) at RT. CV was performed at different scan rates between 10 and 200 $mV \cdot s^{-1}$. GCD was performed at current densities of 0.052 – 1 $mA \cdot cm^{-2}$. The volumetric energy density ($Wh \cdot cm^{-3}$) and power density ($W \cdot cm^{-3}$) were calculated from the volumetric capacitance ($F \cdot cm^{-3}$).[62]

Associated content

Additional data of the synthesis of the ternary composites, EQCM analysis of the control sample rGO-Co_3O_4, details of EIS data analysis and energy density and power density calculations.

Conflict of interest

Authors declare no conflict of interest.

Data Availability

The data supporting this article have been included as part of the Supplementary Information.

Acknowledgements

AB thanks the doctoral school, "Chimie Physique et Chimie Analytique de Paris-Centre" ED388 of Sorbonne University and the French Ministry of Education Scholarship for the financial support. The authors thank Cyrille Bazin for the DRX measurements, Delphine Talbot from Phenix laboratory (Sorbonne Universty, Paris) for TGA analyses and the FabLab of Sorbonne University (Paris, France).

References

1. Wang, S.; Wu, Z.-S.; Zhou, F.; Shi, X.; Zheng, S.; Qin, J.; Xiao, H.; Sun, C.; Bao, X., All-solid-state high-energy planar hybrid micro-supercapacitors based on 2D VN nanosheets and Co(OH)2 nanoflowers. *npj 2D Materials and Applications* **2018,** *2* (1), 7.
2. Dinh, T. M.; Mesnilgrente, F.; Conédéra, V.; Kyerematen, N. A.; Pech, D., Realization of an Asymmetric Interdigitated Electrochemical Micro-Capacitor Based on Carbon Nanotubes and Manganese Oxide. *Journal of The Electrochemical Society* **2015,** *162* (10), A2016.

3. Yue, Y.; Yang, Z.; Liu, N.; Liu, W.; Zhang, H.; Ma, Y.; Yang, C.; Su, J.; Li, L.; Long, F.; Zou, Z.; Gao, Y., A Flexible Integrated System Containing a Microsupercapacitor, a Photodetector, and a Wireless Charging Coil. *ACS Nano* **2016,** *10* (12), 11249-11257.
4. Yuan, Y.; Li, X.; Jiang, L.; Liang, M.; Zhang, X.; Wu, S.; Wu, J.; Tian, M.; Zhao, Y.; Qu, L., Laser maskless fast patterning for multitype microsupercapacitors. *Nat Commun* **2023,** *14* (1), 3967.
5. Jeong, G. H.; Baek, S.; Lee, S.; Kim, S.-W., Metal Oxide/Graphene Composites for Supercapacitive Electrode Materials. *Chemistry – An Asian Journal* **2016,** *11* (7), 949-964.
6. Malik, S.; Gul, I. H.; Baig, M. M., Hierarchical MnNiCo ternary metal oxide/graphene nanoplatelets composites as high rated electrode material for supercapacitors. *Ceramics International* **2021,** *47* (12), 17008-17014.
7. Lakra, R.; Kumar, R.; Sahoo, P. K.; Thatoi, D.; Soam, A., A mini-review: Graphene based composites for supercapacitor application. *Inorganic Chemistry Communications* **2021,** *133*, 108929.
8. Wu, D.; Xie, X.; Zhang, Y.; Zhang, D.; Du, W.; Zhang, X.; Wang, B., MnO2/Carbon Composites for Supercapacitor: Synthesis and Electrochemical Performance. *Frontiers in Materials* **2020,** *7*.
9. Wu, W.; Wei, D.; Zhu, J.; Niu, D.; Wang, F.; Wang, L.; Yang, L.; Yang, P.; Wang, C., Enhanced electrochemical performances of organ-like Ti3C2 MXenes/polypyrrole composites as supercapacitors electrode materials. *Ceramics International* **2019,** *45* (6), 7328-7337.
10. Zhai, S.; Wang, C.; Karahan, H. E.; Wang, Y.; Chen, X.; Sui, X.; Huang, Q.; Liao, X.; Wang, X.; Chen, Y., Nano-RuO2-Decorated Holey Graphene Composite Fibers for Micro-Supercapacitors with Ultrahigh Energy Density. *Small (Weinheim an der Bergstrasse, Germany)* **2018,** *14* (29), 1800582.
11. Fu, M.; Zhuang, Q.; Zhu, Z.; Zhang, Z.; Chen, W.; Liu, Q.; Yu, H., Facile synthesis of V2O5/graphene composites as advanced electrode materials in supercapacitors. *Journal of Alloys and Compounds* **2021,** *862*, 158006.
12. Hui, X.; Qian, L.; Harris, G.; Wang, T.; Che, J., Fast fabrication of NiO@graphene composites for supercapacitor electrodes: Combination of reduction and deposition. *Materials & Design* **2016,** *109*, 242-250.
13. Boychuk, V.; Kotsyubynsky, V.; Rachiy, B.; Bandura, K.; Hrubiak, A.; Fedorchenko, S., β-Ni(OH)2/reduced graphene oxide composite as electrode for supercapacitors. *Materials Today: Proceedings* **2019,** *6*, 106-115.
14. Sun, S.; Li, S.; Wang, S.; Li, Y.; Han, L.; Kong, H.; Wang, P., Fabrication of hollow NiCo2O4 nanoparticle/graphene composite for supercapacitor electrode. *Materials Letters* **2016,** *182*, 23-26.
15. Ke, Q.; Liao, Y.; Yao, S.; Song, L.; Xiong, X., A three-dimensional TiO2/graphene porous composite with nano-carbon deposition for supercapacitor. *Journal of Materials Science* **2016,** *51* (4), 2008-2016.
16. Zhao, Y.; Hao, H.; Song, T.; Wang, X.; Li, C.; Li, W., MnO2-graphene based composites for supercapacitors: Synthesis, performance and prospects. *Journal of Alloys and Compounds* **2022,** *914*, 165343.
17. Qorbani, M.; Chou, T.-c.; Lee, Y.-H.; Samireddi, S.; Naseri, N.; Ganguly, A.; Esfandiar, A.; Wang, C.-H.; Chen, L.-C.; Chen, K.-H.; Moshfegh, A. Z., Multi-porous Co3O4 nanoflakes @ sponge-like few-layer partially reduced graphene oxide hybrids: towards highly stable asymmetric supercapacitors. *Journal of Materials Chemistry A* **2017,** *5* (24), 12569-12577.
18. Lin, G.; Jiang, Y.; He, C.; Huang, Z.; Zhang, X.; Yang, Y., In situ encapsulation of Co3O4 polyhedra in graphene sheets for high-capacitance supercapacitors. *Dalton Transactions* **2019,** *48* (17), 5773-5778.
19. Iqbal, M. Z.; Haider, S. S.; Zakar, S.; Alzaid, M.; Afzal, A. M.; Aftab, S., Cobalt-oxide/carbon composites for asymmetric solid-state supercapacitors. *Materials Research Bulletin* **2020,** *131*, 110974.
20. Zallouz, S.; Réty, B.; Vidal, L.; Le Meins, J.-M.; Matei Ghimbeu, C., Co3O4 Nanoparticles Embedded in Mesoporous Carbon for Supercapacitor Applications. *ACS Applied Nano Materials* **2021,** *4* (5), 5022-5037.
21. Veeresh, S.; Ganesha, H.; Nagaraju, Y. S.; Vijeth, H.; Vandana, M.; Basappa, M.; Devendrappa, H., Graphene oxide/cobalt oxide nanocomposite for high-performance electrode for supercapacitor application. *Journal of Energy Storage* **2022,** *52*, 104715.

22. Wang, H.; Li, W.; Liu, D.; Liu, G.; An, X.; Liu, J.; Zhou, C.; Zhang, H.; Wang, G., Application of Co3O4/Nitrogen-doped carbon composite electrode material derived form Zeolitic imidazolate frameworks-67 in supercapacitors. *Journal of Electroanalytical Chemistry* **2023,** *930*, 117152.
23. Hu, X.; Wei, L.; Chen, R.; Wu, Q.; Li, J., Reviews and Prospectives of Co3O4-Based Nanomaterials for Supercapacitor Application. *ChemistrySelect* **2020,** *5* (17), 5268-5288.
24. Mei, J.; Liao, T.; Ayoko, G. A.; Bell, J.; Sun, Z., Cobalt oxide-based nanoarchitectures for electrochemical energy applications. *Progress in Materials Science* **2019,** *103*, 596-677.
25. Sudhakar, S.; Joshi, D. N.; Peera, S. G.; Sahu, A. K.; Eggleston, C. M.; Prasath, R. A., Hydrothermal-microwave synthesis of cobalt oxide incorporated nitrogen-doped graphene composite as an efficient catalyst for oxygen reduction reaction in alkaline medium. *Journal of Materials Science: Materials in Electronics* **2018,** *29* (8), 6750-6762.
26. Theerthagiri, J.; Thiagarajan, K.; Senthilkumar, B.; Khan, Z.; Senthil, R. A.; Arunachalam, P.; Madhavan, J.; Ashokkumar, M., Synthesis of Hierarchical Cobalt Phosphate Nanoflakes and Their Enhanced Electrochemical Performances for Supercapacitor Applications. *ChemistrySelect* **2017,** *2* (1), 201-210.
27. Meher, S. K.; Rao, G. R., Ultralayered Co3O4 for High-Performance Supercapacitor Applications. *The Journal of Physical Chemistry C* **2011,** *115* (31), 15646-15654.
28. Feng, J.; Zeng, H. C., Size-Controlled Growth of Co3O4 Nanocubes. *Chemistry of Materials* **2003,** *15* (14), 2829-2835.
29. Xu, Y.; Ding, Q.; Li, L.; Xie, Z.; Jiang, G., Facile fabrication of porous Co3O4 nanowires for high performance supercapacitors. *New Journal of Chemistry* **2018,** *42* (24), 20069-20073.
30. Kharade, P. M.; Thombare, J. V.; Babar, A. R.; Bulakhe, R. N.; Kulkarni, S. B.; Salunkhe, D. J., Electrodeposited nanoflakes like hydrophilic Co3O4 as a supercapacitor electrode. *Journal of Physics and Chemistry of Solids* **2018,** *120*, 207-210.
31. Zhou, C.; Zhang, Y.; Li, Y.; Liu, J., Construction of High-Capacitance 3D CoO@Polypyrrole Nanowire Array Electrode for Aqueous Asymmetric Supercapacitor. *Nano Letters* **2013,** *13* (5), 2078-2085.
32. Zhang, X.; Zhang, R.; Xiang, C.; Liu, Y.; Zou, Y.; Chu, H.; Qiu, S.; Xu, F.; Sun, L., Polydopamine-assisted formation of Co3O4-nanocube-anchored reduced graphene oxide composite for high-performance supercapacitors. *Ceramics International* **2019,** *45* (11), 13894-13902.
33. Bathula, C.; Rabani, I.; Ramesh, S.; Lee, S.-H.; Palem, R. R.; Ahmed, A. T. A.; Kim, H. S.; Seo, Y.-S.; Kim, H.-S., Highly efficient solid-state synthesis of Co3O4 on multiwalled carbon nanotubes for supercapacitors. *Journal of Alloys and Compounds* **2021,** *887*, 161307.
34. Jiang, L.; Li, Y.; Luo, D.; Zhang, Q.; Cai, F.; Wan, G.; Xiong, L.; Ren, Z., Freestanding RGO—Co3O4—PPy Composite Films as Electrodes for Supercapacitors. *Energy Technology* **2019,** *7* (3), 1800606.
35. Zhang, S.; Gao, H.; Zhou, J.; Jiang, F.; Zhang, Z., Hydrothermal synthesis of reduced graphene oxide-modified NiCo2O4 nanowire arrays with enhanced reactivity for supercapacitors. *Journal of Alloys and Compounds* **2019,** *792*, 474-480.
36. Su, Y.; Li, S.; Wu, D.; Zhang, F.; Liang, H.; Gao, P.; Cheng, C.; Feng, X., Two-Dimensional Carbon-Coated Graphene/Metal Oxide Hybrids for Enhanced Lithium Storage. *ACS Nano* **2012,** *6* (9), 8349-8356.
37. Tian, J.; Xue, Y.; Wang, M.; Pei, Y.; Zhang, H.; Wang, J., Dopamine constructing composite of Ni(HCO3)2-polydopamine-reduced graphene oxide for high performance electrode in hybrid supercapacitors. *Electrochimica Acta* **2019,** *296*, 49-58.
38. Yan, J.; Lu, H.; Huang, Y.; Fu, J.; Mo, S.; Wei, C.; Miao, Y.-E.; Liu, T., Polydopamine-derived porous carbon fiber/cobalt composites for efficient oxygen reduction reactions. *Journal of Materials Chemistry A* **2015,** *3* (46), 23299-23306.
39. Jiang, J.; Sun, X.; Li, Y.; Deng, C.; Duan, G., Facile synthesis of Fe3O4@PDA core-shell microspheres functionalized with various metal ions: A systematic comparison of commonly-used metal ions for IMAC enrichment. *Talanta* **2018,** *178*, 600-607.

40. Luo, F.; Wu, K.; Shi, J.; Du, X.; Li, X.; Yang, L.; Lu, M., Green reduction of graphene oxide by polydopamine to a construct flexible film: superior flame retardancy and high thermal conductivity. *Journal of Materials Chemistry A* **2017,** *5* (35), 18542-18550.
41. Dong, S.; Xie, Z.; Fang, Y.; Zhu, K.; Gao, Y.; Wang, G.; Yan, J.; Cheng, K.; Ye, K.; Cao, D., Polydopamine-Modified Reduced Graphene Oxides as a Capable Electrode for High-Performance Supercapacitor. *ChemistrySelect* **2019,** *4* (9), 2711-2715.
42. Liu, Y.; Weng, B.; Xu, Q.; Hou, Y.; Zhao, C.; Beirne, S.; Shu, K.; Jalili, R.; Wallace, G. G.; Razal, J. M.; Chen, J., Facile Fabrication of Flexible Microsupercapacitor with High Energy Density. *Advanced Materials Technologies* **2016,** *1* (9), 1600166.
43. Wang, Y.; Zhao, Y.; Qu, L., Laser fabrication of functional micro-supercapacitors. *Journal of Energy Chemistry* **2021,** *59*, 642-665.
44. Yoo, J.; Byun, S.; Lee, C.-W.; Yoo, C.-Y.; Yu, J., Precisely Geometry Controlled Microsupercapacitors for Ultrahigh Areal Capacitance, Volumetric Capacitance, and Energy Density. *Chemistry of Materials* **2018,** *30* (12), 3979-3990.
45. Bouzina, A.; Meng, R.; Pillier, F.; Perrot, H.; Sel, O.; Debiemme-Chouvy, C., Hydrothermal synthesis of a graphene-based composite enabling the fabrication of a current collector-free microsupercapacitor with improved energy storage performance. *Batteries & Supercaps n/a* (n/a), e202300430.
46. Thangavelu, K.; Parameswari, K.; Kuppusamy, K.; Haldorai, Y., A simple and facile method to synthesize Co3O4 nanoparticles from metal benzoate dihydrazinate complex as a precursor. *Materials Letters* **2011,** *65* (10), 1482-1484.
47. Kim, K. S.; Park, Y. J., Catalytic properties of Co3O4 nanoparticles for rechargeable Li/air batteries. *Nanoscale Research Letters* **2012,** *7* (1), 47.
48. Sauerbrey, G., Verwendung von Schwingquarzen zur Wägung dünner Schichten und zur Mikrowägung. *Zeitschrift für Physik* **1959,** *155* (2), 206-222.
49. Bouzina, A.; Perrot, H.; Sel, O.; Debiemme-Chouvy, C., Preventing Graphene from Restacking via Bioinspired Chemical Inserts: Toward a Superior 2D Micro-supercapacitor Electrode. *ACS Applied Nano Materials* **2021,** *4* (5), 4964-4973.
50. Gao, W.; Krins, N.; Laberty-Robert, C.; Perrot, H.; Sel, O., Scrutiny of the LiCoO2 Composite Electrode/Electrolyte Interface by Advanced Electrogravimetry and Implications for Aqueous Li-Ion Batteries. *The Journal of Physical Chemistry C* **2021,** *125* (7), 3859-3867.
51. Muramatsu, H.; Egawa, A.; Ataka, T., Reliability of correlation between mass change and resonant frequency change for a viscoelastic-film-coated quartz crystal. *Journal of Electroanalytical Chemistry* **1995,** *388* (1), 89-92.
52. Xiang, C.; Wang, Q.; Zou, Y.; Huang, P.; Chu, H.; Qiu, S.; Xu, F.; Sun, L., Simple synthesis of graphene-doped flower-like cobalt–nickel–tungsten–boron oxides with self-oxidation for high-performance supercapacitors. *Journal of Materials Chemistry A* **2017,** *5* (20), 9907-9916.
53. Bouzina, A.; Meng, R.; Bazin, C.; Perrot, H.; Sel, O.; Debiemme-Chouvy, C., Highly Ordered Graphene Polydopamine Composite Allowing Fast Motion of Cations: Toward a High-Performance Microsupercapacitor. *Advanced Materials Interfaces* **2023,** *10* (32), 2300442.
54. Ma, J.; Zheng, S.; Cao, Y.; Zhu, Y.; Das, P.; Wang, H.; Liu, Y.; Wang, J.; Chi, L.; Liu, S.; Wu, Z.-S., Aqueous MXene/PH1000 Hybrid Inks for Inkjet-Printing Micro-Supercapacitors with Unprecedented Volumetric Capacitance and Modular Self-Powered Microelectronics. *Advanced Energy Materials* **2021,** *11* (23), 2100746.
55. Jayaraman, P.; Annal Therese, H., Flexible interdigitated symmetric solid-state micro-supercapacitors with higher energy density for wearable electronics. *Journal of Power Sources* **2023,** *581*, 233489.
56. Rong, Y.; Chen, Y.; Zheng, J.; Zhao, Y.; Li, Q., Development of high performance alpha-Co(OH)2/reduced graphene oxide microfilm for flexible in-sandwich and planar micro-supercapacitors. *Journal of Colloid and Interface Science* **2021,** *598*, 1-13.

57. Feng, X.; Ning, J.; Wang, D.; Zhang, J.; Dong, J.; Zhang, C.; Shen, X.; Hao, Y., All-solid-state planner micro-supercapacitor based on graphene/NiOOH/Ni(OH)2 via mask-free patterning strategy. *Journal of Power Sources* **2019,** *418*, 130-137.
58. Liu, W.; Lu, C.; Wang, X.; Tay, R. Y.; Tay, B. K., High-Performance Microsupercapacitors Based on Two-Dimensional Graphene/Manganese Dioxide/Silver Nanowire Ternary Hybrid Film. *ACS Nano* **2015,** *9* (2), 1528-1542.
59. Lee, S. H.; Lee, J.; Jung, J.; Cho, A. R.; Jeong, J. R.; Dang Van, C.; Nah, J.; Lee, M. H., Enhanced Electrochemical Performance of Micro-Supercapacitors Via Laser-Scribed Cobalt/Reduced Graphene Oxide Hybrids. *ACS Applied Materials & Interfaces* **2021,** *13* (16), 18821-18828.
60. Naderi, L.; Shahrokhian, S., Wire-type flexible micro-supercapacitor based on MOF-assisted sulfide nano-arrays on dendritic CuCoP and V2O5-polypyrrole/nanocellulose hydrogel. *Chemical Engineering Journal* **2023,** *476*, 146764.
61. Bizet, K.; Gabrielli, C.; Perrot, H., Immunodetection by quartz crystal microbalance - A new approach for direct detection of rabbit IgG and peroxidase. *Applied Biochemistry and Biotechnology* **2000,** *89* (2-3), 139-149.
62. Simon, P.; Gogotsi, Y., Perspectives for electrochemical capacitors and related devices. *Nature Materials* **2020,** *19* (11), 1151-1163.

SUPPORTING INFORMATION

Current collector-free symmetric μ-supercapacitor device based on a ternary composite of graphene, polydopamine and Co_3O_4

Adnane Bouzina[1], René Meng[1], Françoise Pillier[1], Hubert Perrot[1], Catherine Debiemme-Chouvy[1,*] and Ozlem Sel[2,3,*]

[1] Sorbonne Université, CNRS, Laboratoire Interfaces et Systèmes Electrochimiques, LISE UMR 8235, 4 place Jussieu, F-75005 Paris, France

[2] Chimie du Solide et de l'Energie, UMR 8260, Collège de France, 11 place Marcelin Berthelot, F-75231 Paris Cedex 05, France

[3] Réseau sur le Stockage Electrochimique de l'Energie (RS2E), CNRS FR 3459, 33 rue Saint Leu, F-80039 Amiens Cedex, France

Part I. Synthesis and characterization of materials

Table S1. Experimental conditions for preparing the rGO-PDA-Co_3O_4 composites with different GO/Co ratios.

Composite powder	Mass (g) $CoCl_2•6H_2O$	Mass ratio GO/$CoCl_2•6H_2O$	Mass ratio GO/DA
rGO-PDA-Co_3O_4 (1)	0.3	5 %	50 %
rGO-PDA-Co_3O_4 (2)	0.15	10 %	50 %
rGO-PDA-Co_3O_4 (3)	0.1	15 %	50 %

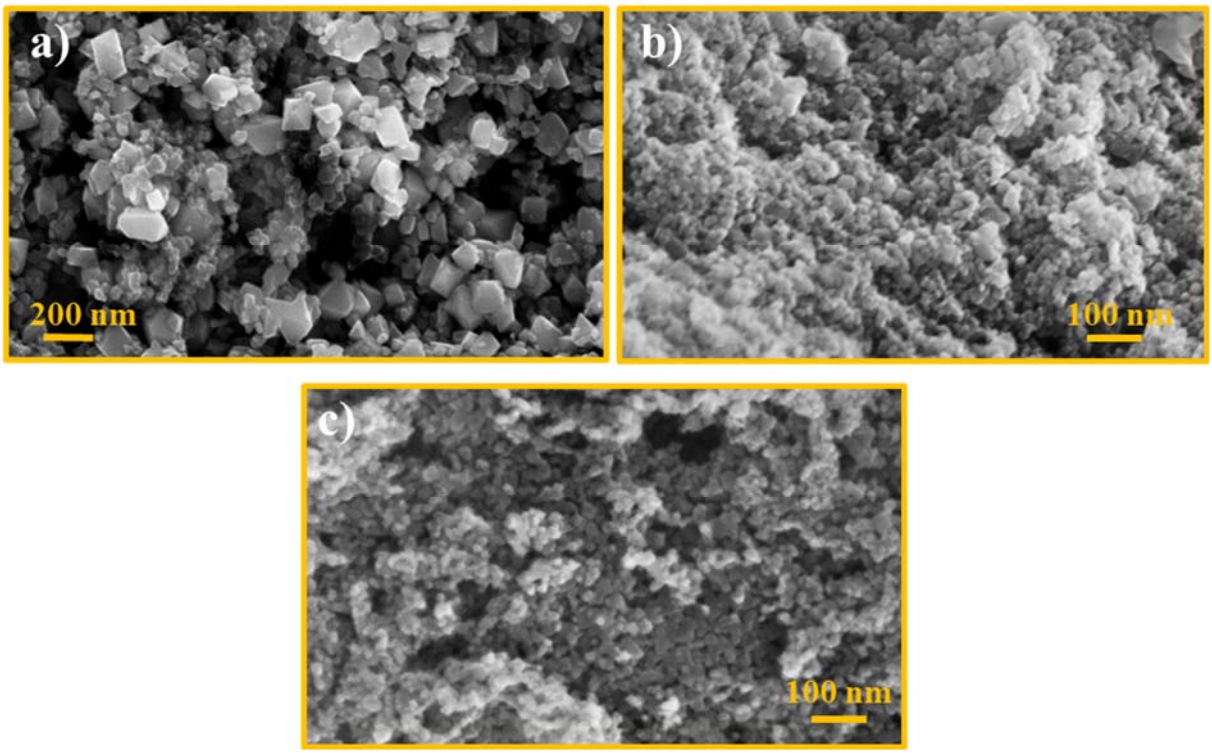

Figure S1. SEM micrographs of the (a) Co_3O_4, (b) rGO-Co_3O_4 and (c) rGO-PDA-Co_3O_4 powders after calcination at 500 °C for 2h.

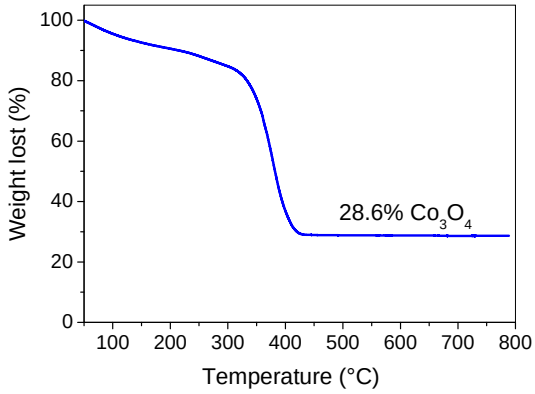

Figure S2. Thermal gravimetric analysis of rGO-PDA-Co_3O_4, under air; at 10 °C/min.

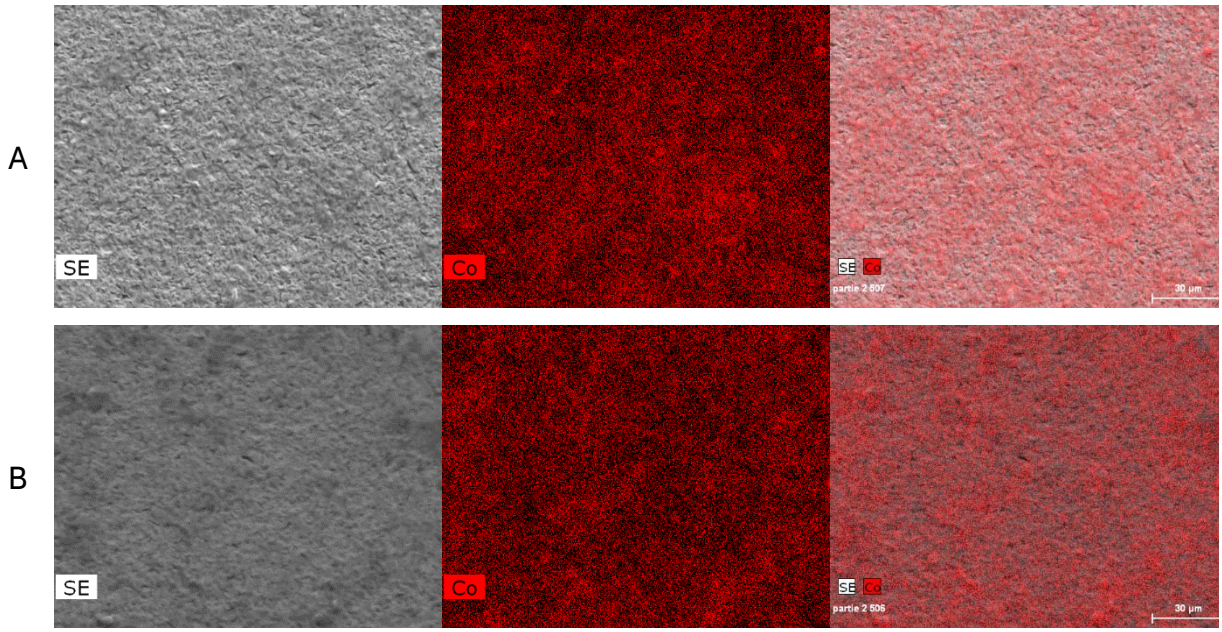

Figure S3. Cobalt elemental analysis by the EDX analysis of the SEM micrographs (SE) of A) rGO-Co_3O_4 and B) rGO-PDA-Co_3O_4 thin films.

Table S2. Thicknesses estimated by SEM, deposited mass and density of rGO-Co_3O_4 and rGO-PDA-Co_3O_4 films.

Material	Average thickness (nm)	Mass estimated by QCM (µg)	Density (g/cm^3)
rGO-Co_3O_4	380	11.7	1.55
rGO-PDA-Co_3O_4	430	13.6	1.58

Part II. Electrochemical and electrogravimetric analyses

Gravimetric EQCM analysis

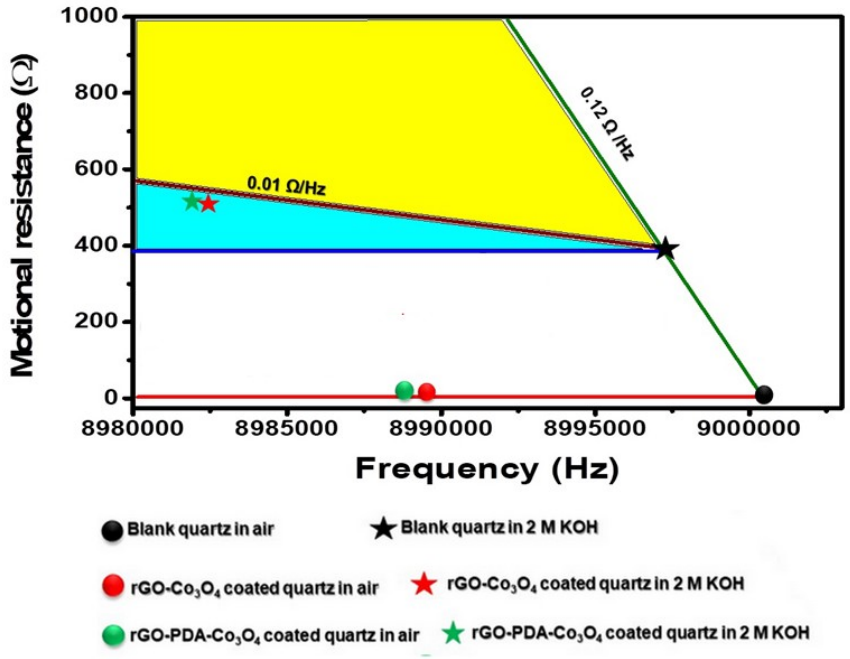

Figure S4. Evolution of motional resistance as a function of resonance frequency in air and in a KOH solution (2 M) for rGO-Co_3O_4 and rGO-PDA-Co_3O_4 films deposited on a Au electrode of a quartz resonator.

Electrochemical cycling in aqueous electrolytes

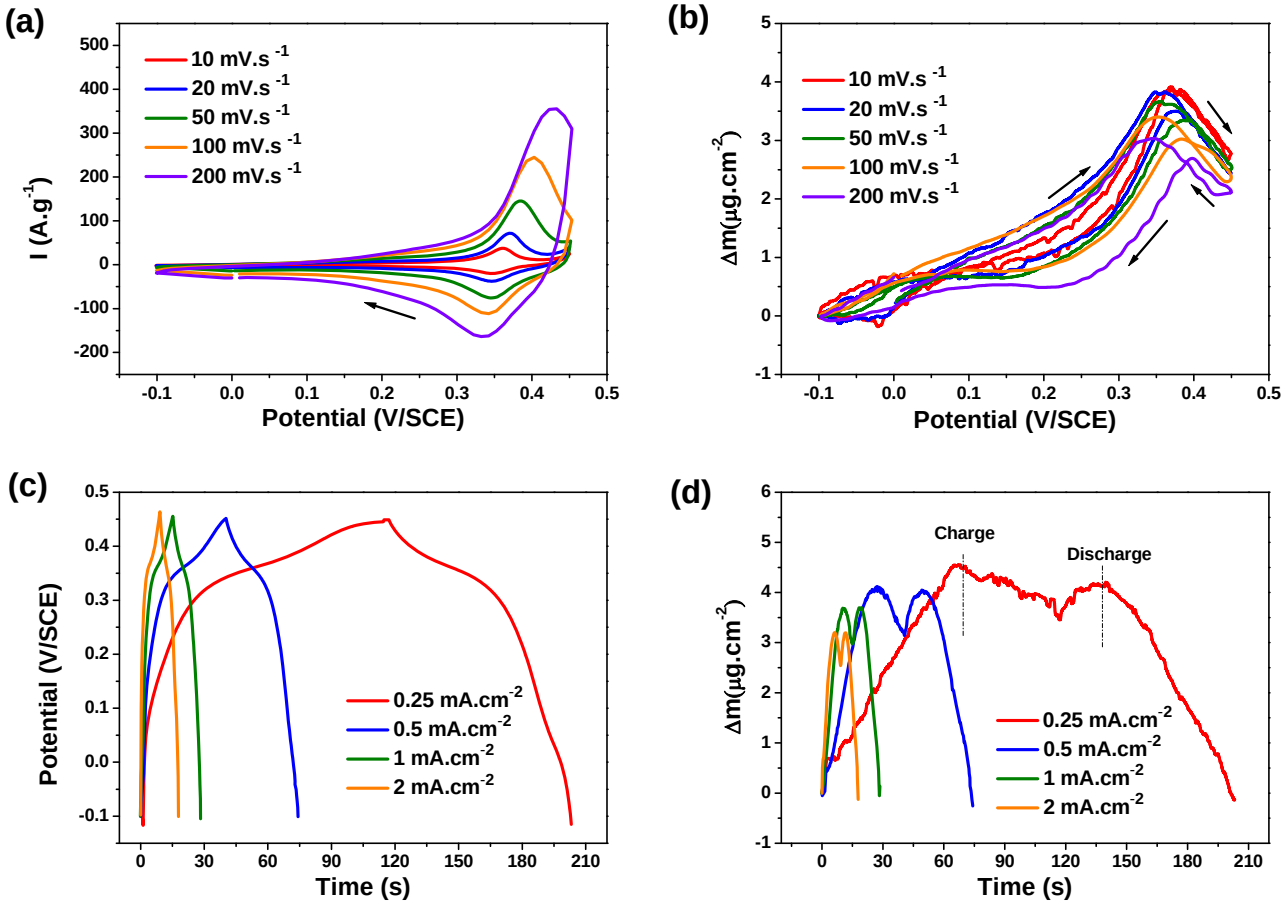

Figure S5. a) Cyclic voltammograms and b) mass variation as a function of potential for rGO-Co_3O_4 at different scan rates, in 2 M KOH. c) Potential variation as a function of time and d) the corresponding variation of mass for rGO-Co_3O_4, during galvanostatic charge/discharge at different current densities, in 2 M KOH.

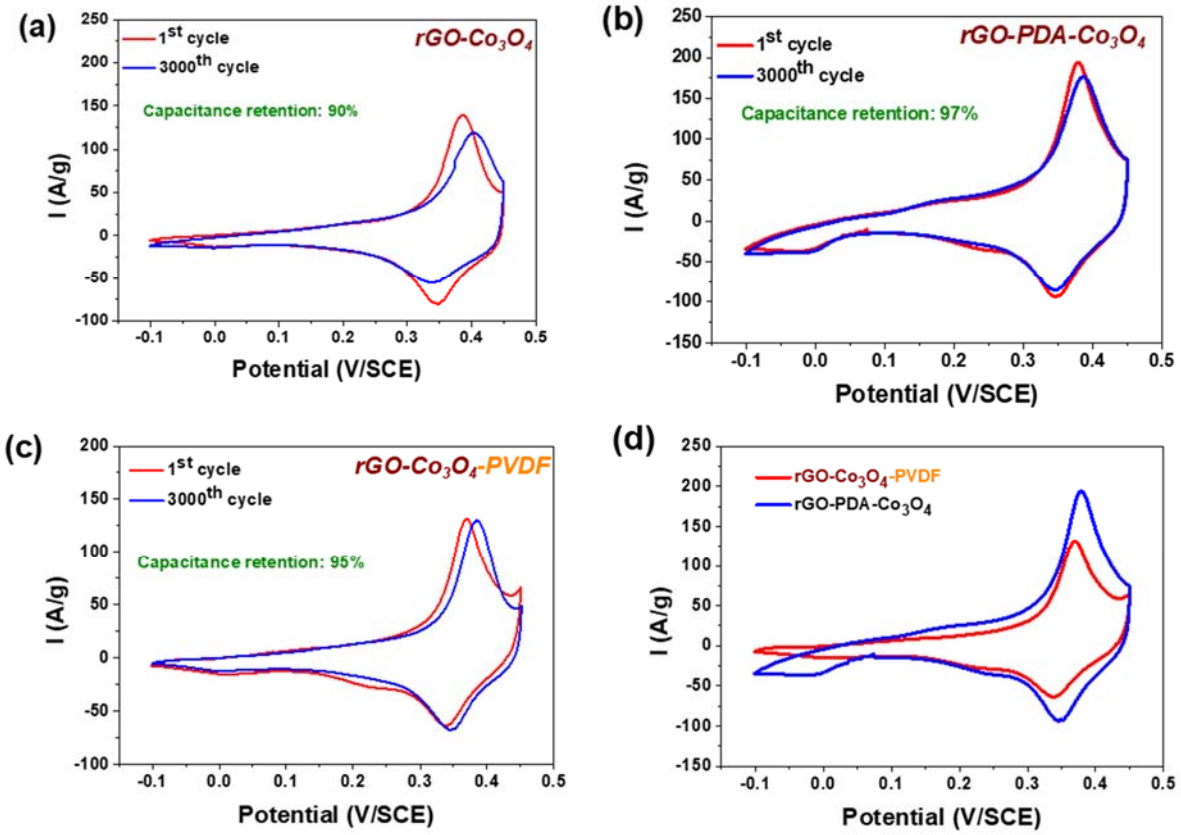

Figure S6. Cycling stability of (a) rGO-Co_3O_4, (b) rGO-PDA-Co_3O_4 and (c) rGO-Co_3O_4-PVDF. (d) Comparison of cyclic voltammograms of rGO-PDA-Co_3O_4 and rGO-Co_3O_4-PVDF (1st cycle), in 2 M KOH, at a scan rate of 50 $mV \cdot s^{-1}$.

Electrochemical impedance spectroscopy and complex capacitance calculations

Specific capacitances are generally obtained from galvanostatic charge/discharge cycles or cyclic voltammetry. However, for EDLC electrodes, capacitance is frequency-dependent, and can be determined by electrochemical impedance spectroscopy according to the complex capacitance model:

$$C(\omega) = C'(\omega) + jC''(\omega) \quad \textbf{(S1)}$$

$$C'(\omega) = \frac{-Z''(\omega)}{\omega |Z(\omega)|^2} \quad \textbf{(S2)}$$

$$C''(\omega) = \frac{Z'(\omega)}{\omega |Z(\omega)|^2} \quad \textbf{(S3)}$$

where Z′, Z″, and Z are the real, imaginary, and total impedance values, respectively, in ohms with $j^2 = -1$. The entities C′, C″, and C represent the real part, imaginary part and total capacitance, respectively, at a given frequency.

From the curve representing $C''(\omega)$ it is possible to determine the relaxation time which corresponds to the frequency (f_0) of the peak of the $C''(\omega)$ response:

$$\tau_0 = \frac{1}{f_0} \quad \textbf{(S4)}$$

The time constant (τ_0) is characteristic of the rapidity of the system response (charge-discharge kinetics).

Energy density and power density calculations from GCD test

The energy density (E) and the power density (P) of a microsupercapacitor are calculated from the GCD curve according to Equation S5 and S6.

$$E = \frac{C_V \, \Delta V^2}{2 \; x \; 3600} \quad \textbf{(S5)}$$

$$P = \frac{3600 \, E}{\Delta t} \quad \textbf{(S6)}$$

where C_V is the volumetric capacitance, ΔV represents the voltage window, and Δt is the discharge time.